Epoxy Nanocomposites Based on the Synthetic α-Zirconium Phosphate Layer Structure

H.-J. Sue* and K. T. Gam

Polymer Technology Center, Department of Mechanical Engineering, Texas A&M University, College Station, Texas 77843-3123

N. Bestaoui, N. Spurr, and A. Clearfield*

Department of Chemistry, Texas A&M University, College Station, Texas 77843-3255

Received June 23, 2003. Revised Manuscript Received November 3, 2003

The morphology and mechanical properties of epoxy nanocomposites based on synthetic α-zirconium phosphate (α-ZrP) layer structure have been investigated. The interlayer surfaces of α-ZrP can be easily modified because of its high surface ion exchange capacity characteristics. The α-ZrP structure is layered claylike and possesses aspect ratios of at least 100. The state of exfoliation has been confirmed using direct transmission electron microscopy observation at various locations of the sample. With an addition of only 1.9 vol % α-ZrP, the tensile modulus of the α-ZrP-reinforced epoxy nanocomposite is increased by 50%, and the yield strength improved by 10%. However, the ductility of the matrix (elongation at break) is drastically reduced after the α-ZrP reinforcement. The fundamental structure−property relationship of α-ZrP-based epoxy nanocomposite is discussed.

Introduction

Polymer nanocomposites exhibit significantly better physical and mechanical properties than conventional micrometer-scale inorganic filler reinforced polymer composites.[1−21] Polymer nanocomposites with matrixes based on epoxy,[1−7] polyamide-6,[8−15] polypropylene (PP),[16,17] and polystyrene[18] and nanofillers based on montmorillonite clay, TiO_2, $CaCO_3$, and SiO_2,[19−21] have been extensively studied. Significant efforts have been paid to achieve maximum dispersion of nanofillers in polymer matrixes. However, aggregation of nanofillers, to various degrees, is unavoidable. As a result, the cause(s) for the significant drops in ductility and toughness found in polymer nanocomposites cannot be unambiguously determined to be due to the constraining effect of the nanofiller particles or to the presence of the detrimental aggregates in the polymer matrix, or both.

Montmorillonite clay is among the most widely chosen nanofiller for polymer nanocomposites because of its several advantages. Clays have high ion exchange capacity, which allows modification of the interlayer spacing to achieve better compatibility with host polymer matrixes. It also exhibits high aspect ratio to give better reinforcement effect.[22] Most importantly, clay is abundant and inexpensive. Its potential for large-scale commercial uses is high. In general, clay-based nanocomposites exhibit greatly enhanced modulus and gas barrier properties of the host polymers,[1−15] but cause significant reduction in ductility and toughness.

The main drawback of montmorillonite clay is that it is produced via purification and modification of the mined clay. It is extremely difficult, if not impossible,

* Authors to whom correspondence should be addressed. H. Sue: tel., (979) 845-5024; fax, (979) 862-3989; e-mail, hjsue@tamu.edu. A. Clearfield: e-mail, clearfield@mail.chem.tamu.edu.

(1) (a) Wang, Z.; Pinnavaia, T. J. *Chem. Mater.* **1998**, *10*, 1820. (b) Messersmith, P. B.; Giannelis, E. P. *Chem. Mater.* **1994**, *6*, 1719.
(2) Massam, J.; Pinnavaia, T. J. *Mater. Res. Soc. Symp. Proc.* **1998**, *520*, 223.
(3) Shi, H. Z.; Lan, T.; Pinnavaia, T. J. *Chem. Mater.* **1996**, *8*, 1584.
(4) Wang, Z.; Lan, T.; Pinnavaia, T. J. *Chem. Mater.* **1996**, *8*, 2200.
(5) (a) Lan, T.; Kaviratna, P. D.; Pinnavaia, T. J.; *Chem. Mater.* **1995**, *7*, 2144. (b) Burnside, S. D.; Gianelis, E. P. *Chem. Mater.* **1995**, *7*, 1597.
(6) Pinnavaia, T. J.; Lan, T.; Kaviratna, P. D.; Wang, M. S. *Mater. Res. Soc. Symp. Proc.* **1994**, *346*, 81.
(7) Gam, K. T.; Miyamoto, T.; Nishimura, R.; Sue, H.-J. *Polym. Eng. Sci.*, in press.
(8) Kojima, Y.; Usuki, A.; Kawasumi, M.; Okada, A.; Fukushima, Y.; Kurauchi, T.; Kamigaito, O. *J. Mater. Res.* **1993**, *8*, 1185.
(9) Masenelli-Varlot, K.; Reynaud, E.; Vigier, G.; Varlet, J. *J. Polym. Sci., Part B: Polym. Phys.* **2002**, *40*, 272.
(10) Wang, H.; Zeng, C. C.; Elkovitch, M.; Lee, L. J.; Koelling, K. W. *Polym. Eng. Sci.* **2001**, *41*, 2036.
(11) Fornes, T. D.; Yoon, P. J.; Keskkula, H.; Paul, D. R. *Polymer* **2001**, *42*, 9929.
(12) Liu, L. M.; Qi, N.; Zhu, X. G. *J. Appl. Polym. Sci.* **1999**, *71*, 1133.
(13) Kojima, Y.; Usuki, A.; Kawasumi, M.; Okada, A.; Kurauchi, T.; Kamigaito, O. *J. Polym. Sci., Part A: Polym. Chem.* **1993**, *31*, 983.
(14) Kojima, Y.; Usuki, A.; Kawasumi, M.; Okada, A.; Kurauchi, T.; Kamigaito, O. *J. Polym. Sci., Part A: Polym. Chem.* **1993**, *31*, 1755.
(15) Kojima, Y.; Usuki, A.; Kawasumi, M.; Okada, A.; Fukushima, Y.; Kurauchi, T.; Kamigaito, O. *J. Mater. Res.* **1993**, *8*, 1185.
(16) Hasegawa, N.; Kawasumi, M.; Kato, M.; Usuki, A.; Okada, A. *J. Appl. Polym. Sci.* **1998**, *67*, 87.
(17) Wang, H.; Zeng, C. C.; Elkovitch, M.; Lee, L. J.; Koelling, K. W. *Polym. Eng. Sci.* **2001**, *41*, 2036.
(18) Hasegawa, N.; Okamoto, H.; Kawasumi, M.; Usuki, A. *J. Appl. Polym. Sci.* **1999**, *74*, 3359.
(19) Ng, C. B.; Ash, B. J.; Schadler, L. S.; Siegel, R. W. *Adv. Comput. Lett.* **2001**, *10*, 101.
(20) Chan, C. M.; Wu, J. S.; Li, J. X.; Cheung, Y. K. *Polymer* **2002**, *43*, 2981.
(21) Rong, M. Z.; Zhang, M. Q.; Zheng, Y. X.; Zeng, H. M.; Walter, R.; Friedrich, K. *Polymer* **2001**, *42*, 167.
(22) Borchardt, G. Smectites. In *Minerals in Soil Environments*; Dixon, J. B., Weed, S. B., Eds.; Soil Science Society of America: Madison, WI, 1989; Chapter 14, p 675.

10.1021/cm030441s CCC: $27.50
Published on Web 12/18/2003

to achieve 100% purity, narrow particle size distribution, and controlled aspect ratio of the clay nanofiller. With the exception of nylon 6/clay nanocomposites,[23] most of the published results on clay-based polymer nanocomposites only exhibit incomplete exfoliation of the clay.[24−26] Many of the inconsistent claims on how nanofillers influence properties, such as T_g, toughness, ductility, and strength, may partially be due to imperfect exfoliation or presence of aggregation of clay in the polymer matrix, or some unknown nanofiller surface chemistry and reactions. Consequently, despite the significant research efforts in the past 2 decades, fundamental knowledge on exactly how the degree of dispersion, aspect ratio, and particle size of nanoparticles influence the physical and mechanical properties of polymers is still lacking. It is imperative to prepare model polymer nanocomposites that contain nanofillers with controlled surface functionalities, particle sizes, and aspect ratios to gain unambiguous fundamental understanding of mechanical behavior of polymer nanocomposites.

Stemming from the above concerns, as a part of a larger effort to gain fundamental structure−property relationship in polymer nanocomposites, we used α-zirconium phosphate (α-ZrP), $Zr(HPO_4)_2 \cdot H_2O$, as a nanofiller in this study. α-ZrP has a much higher ion exchange capacity than montmorillonite clays, and the size and aspect ratio of the α-ZrP particles can be controlled by varying reaction time and reactant concentrations.[27] Also, the particle size distribution of α-ZrP has been found to be quite narrow, thus suitable for fundamental study of nanofiller effect on the properties of the host polymers.

Crystalline α-ZrP was first prepared in 1964 by Clearfield and Stynes.[28] The crystal structure has been determined to be a layer structure in both $P2_1/n$ and $P2_1/c$ space groups.[29] This layer structure is similar to that of montmorillonite clay. However, the layers are formed by zirconium atoms connected between them by the oxygen atoms of the phosphate groups. Each phosphate contributes three of its oxygen atoms to the formation of these layers, leaving one OH group pointing into the interlayer space. Earlier studies have shown that α-ZrP is capable of incorporating 2 mol of *n*-alkylamines with the formation of a bilayer in the interlayer space.[30] This occurs through an acid−base reaction, where the proton is transferred from the −POH group to the nitrogen or by hydrogen bonding.

So far, only two related research papers were found focusing on the intercalation of α-ZrP particles using amino acids[31] and on α-ZrP modification using equimolar tetra-*n*-butylammonium hydroxide to prepare thin films of α-ZrP.[32] No known effort has been focused on the utilization of α-ZrP to prepare polymer nanocomposites.

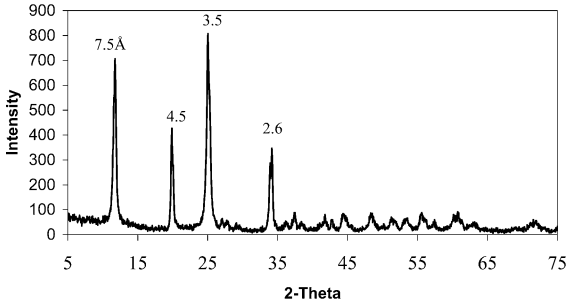

Figure 1. X-ray powder pattern of α-zirconium phosphate prepared in 3 M H_3PO_4. The interlayer spacing is 7.6 Å.

In this study, α-ZrP with a large interlayer spacing was synthesized to make α-ZrP/epoxy nanocomposites. For this purpose α-ZrP was intercalated using a commercially available monoamine-terminated polyether, Jeffamine M715 (M715), with the formula $CH_3O(CH_2CH_2O)_{14}CH_2CH_2NH_2$. The resulting material is then incorporated into an epoxy polymer. The morphology and mechanical properties of the α-ZrP−reinforced epoxy nanocomposites are studied. The influence of α-ZrP nanoparticles on physical and mechanical properties enhancement of epoxy matrix is investigated. The implication of this research on fundamental understanding of physical, mechanical, and functional properties of polymer nanocomposites is also discussed. A preliminary report as a proceedings account is available.[33]

Experimental Section

Materials. The reagents were used as-received: Zirconium oxychloride octahydrate ($ZrOCl_2 \cdot 8H_2O$), 98% (Aldrich), phosphoric acid (EM), Jeffamine M715 (Huntsman Chemical), and methyl ethyl ketone (Merck). Diglycidyl ether of bisphenol A (DGEBA) epoxy resin (DER 332, Dow Chemical) was mixed with 4,4′-diamino-diphenyl sulfone (DDS, Aldrich), which is a curing agent, as the epoxy matrix for this study. The DGEBA epoxy monomer has a narrow monomer molecular weight distribution of 172−176 g/mol.

Synthesis. *Preparation of α-ZrP.* The detailed chemistry and procedures for the preparation for α-ZrP can be found elsewhere.[34] Only a brief summary of the α-ZrP preparation is given here. A gel was prepared by the addition of $ZrOCl_2 \cdot 8H_2O$ to phosphoric acid and then refluxed 24 h in 3 M phosphoric acid solution. The X-ray powder pattern of this compound is presented in Figure 1. The broadened peaks show that the compound is not perfectly crystallized because the acid used is dilute. The interlayer spacing of this compound is about 7.6 Å. The scanning electron micrograph (Figure 2) shows the formation of aggregates, which consist of many irregular small particles. The sizes of the aggregated particles vary between 0.3 and 2 μm.

Intercalation of α-ZrP with Jeffamine M715. The intercalation reaction[35] of α-ZrP was carried out at room temperature. Twenty millimoles of α-ZrP powder was dispersed in 100 mL of methyl ethyl ketone (MEK) for 6 h. Forty millimoles of

(23) Usuki, A.; Kojima, Y.; Kawasumi, M.; Okada, A.; Fukushima, Y.; Kurauchi, T.; Kamigaito, O. *J. Mater. Res.* **1993**, *8*, 1179.
(24) Wang, M. S.; Pinnavaia, T. *Chem. Mater.* **1994**, *6*, 468.
(25) Lan, T.; Pinnavaia, T. *Chem. Mater.* **1994**, *6*, 2216.
(26) Kurokawa, Y.; Yasuda, H.; Kashiwagi, M.; Oyo, A. *J. Mater. Sci. Lett.* **1997**, *16*, 1670.
(27) Clearfield, A. *Annu. Rev. Mater. Sci.* **1984**, *14*, 205.
(28) Clearfield, A.; Stynes, J. A. *J. Inorg. Nucl. Chem.* **1964**, *26*, 117.
(29) Clearfield, A.; Smith, G. D. *Inorg. Chem.* **1969**, *8*, 431. Troup, J. M.; Clearfield, A. *Inorg. Chem.* **1977**, *16*, 3311.
(30) Clearfield, A.; Tindwa, R. M. *J. Inorg. Nucl. Chem.* **1979**, *41*, 871.
(31) Ding, Y.; Jones, D. J.; Maireles-Torres, P.; Roziere, J. *Chem. Mater.* **1995**, *7*, 562.
(32) Kim, H.; Keller, S. W.; Mallouk, T. E.; Schmitt, J.; Decher, G. *Chem. Mater.* **1997**, *9*, 1414.
(33) Gam, K. T.; Bestaoui, N.; Spurr; N.; Clearfield, A.; Sue, H.-J. *Soc. Plastics Eng.* **2003**, 61 (Vol. 2), 1434.
(34) (a) Clearfield, A., Duax, W. L.; Medina, A. S.; Smith, G. O.; Thomas, J. R. *J. Phys. Chem.*, **1969**, *73*, 3424. (b) Clearfield, A.; Oskarsson, A.; Oskarsson, C. *Ion Exch. Membr.* **1972**, *1*, 91.
(35) Bestaoui, N.; Spurr N.; Clearfield, A. Submitted to *Chem. Mater.*

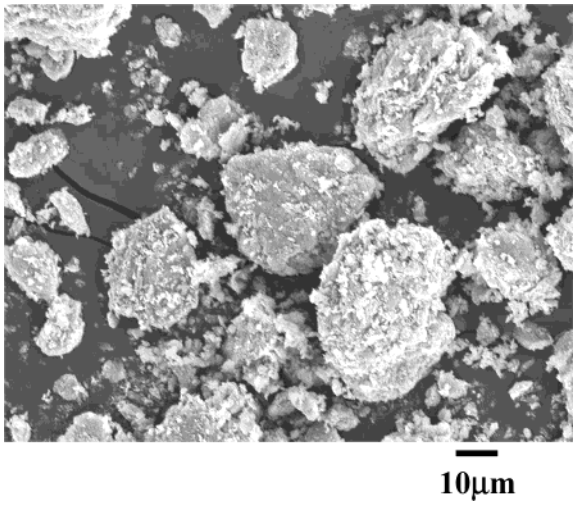

Figure 2. Electron scanning micrographs of α-zirconium phosphate at a magnification of 800. This compound is constituted of aggregates with particle sizes varying between 2 and 0.3 μm.

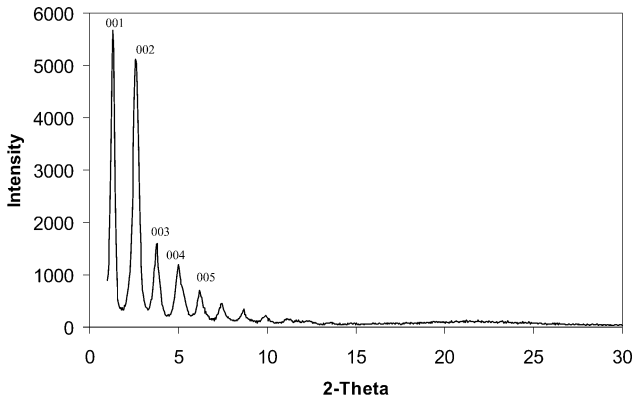

Figure 3. X-ray powder pattern of α-zirconium phosphate intercalated with Jeffamine M715. The layered character of the compound is observed. The interlayer spacing is 73.27 Å.

monoamine surface modifier (M715) was first dissolved in 100 mL of MEK and then added dropwise into the α-ZrP/MEK mixture. A transparent yellowish "gel" was obtained. It was not possible to wash off the excess monoamine modifier and to dry the resulting compound completely due to its gelatinous nature. The X-ray diffraction powder pattern of the intercalated α-ZrP (M-α-ZrP) is presented in Figure 3.

Preparation of α-ZrP-Based Epoxy Nanocomposites. The M-α-ZrP was poured into the epoxy to achieve 1.9 vol % (5.2 wt %) of α-ZrP in epoxy (M-α-ZrP/epoxy). After removal of MEK with a Rotavapor in a water bath at about 90 °C under vacuum, no aggregation or precipitation was found in the viscous mixture. The mixture was then heated at 130 °C, and the curing agent, DDS, was added at stoichiometric ratio. This mixture was stirred until a transparent yellowish solution was obtained. The mixture was degassed under vacuum and poured into a preheated glass mold. A plaque with dimensions 200 mm (8 in.) × 200 mm (8 in.) × 3.12 mm (0.125 in.) was cast. The resin mixture was cured in an oven at 180 °C for 2 h, followed by 2 h of post-cure at 220 °C.

For comparison, a neat epoxy panel (neat/epoxy), an epoxy panel with only the Jeffamine (M/epoxy), and an epoxy panel (α-ZrP/epoxy) with 1.9 vol % of α-ZrP were prepared. The density of α-ZrP is much higher than DGEBA epoxy; the α-ZrP particles were dispersed in MEK and stirred overnight to achieve good dispersion in the resin matrix. Then, the mixture was blended with DGEBA and the same procedure as above was followed. Table 1 presents the composition in vol % of the different panels.

Table 1. Compositions (vol %)

	α-zirconium phosphate	Jeffamine M715
neat (DGEBA/DDS)	none	none
M/epoxy	none	18.7
α-ZrP/epoxy	1.9	none
M-α-ZrP/epoxy	1.9	18.7

Characterization. X-ray diffraction powder patterns were recorded using a Bruker D8 diffractometer with Bragg−Brentano $\theta-2\theta$ geometry (40 kV and 40 mA) and a graphite monochromator. The data were recorded between 1° and 30° in 2θ, with a step increment of 0.04° and a count time of 2 s per step for the intercalated compound and the polymers. For the M-α-ZrP, the samples were prepared by putting a drop of the mixture on the surface of a flat holder. By slow evaporation of the solvent, a thin film was formed on the surface of the holder for analysis. For α-ZrP the data were taken between 5° and 75° in 2θ, with a step size of 0.04° and a count time of 2s per step. The powder was packed into a plastic holder.

The solid-state NMR was performed with magic-angle spinning (MAS) on a modified Bruker MSL-300 MHz machine, operating at 121.5 MHz for ^{31}P. Eighty five percent H_3PO_4 (0 ppm) was used as an external standard.

The infrared spectra were recorded on a Nicolet Nexus 470 FTIR spectrometer with a spectral resolution of 2.000 cm^{-1}. A small amount of the sample was put between two blocks of KBr for analysis. Optical microscopy (OM) was performed using an Olympus optical microscope (model BX60) under both bright field and crossed polars. Scanning electron microscopy (SEM) investigations were performed (on the fracture surface of the SEN-3PB specimen) using a JEOL JSM-6400, operated at 20 kV (to observe the overall α-ZrP particle distribution and the homogeneity of the dispersion in epoxy). Transmission electron microscopy (TEM) was performed on a JEOL JEM-2010A, operated at 200 kV. A Reichert-Jung Ultracut-E microtome was utilized to prepare thin sections with 70−100 nm in thickness for TEM observation.

Mechanical Property Characterization. Dynamic mechanical analysis (DMA) was performed using a Rheometrics (RDS-II) at a fixed frequency of 1 Hz and a temperature sweep of 5 °C per step, ranging from −150 to 250 °C. A sinusoidal strain-amplitude of 0.10% was chosen for the analysis. The dynamic storage modulus (G') and tan δ against temperature curves were recorded and plotted. The temperature at which the tan δ curve shows a maximum peak is recorded as the glass transition temperature (T_g).

A tensile test (ASTM D638-98) was performed using a screw-driven mechanical testing machine (Sintech-2) at a crosshead speed of 0.508 mm/min (0.2 in./min) at room temperature. An average of at least five tests per sample was performed to report modulus, yield stress, and elongation at break. The fracture toughness measurements of the α-ZrP-based epoxy nanocomposites were conducted based on the linear elastic fracture mechanics (LEFM) approach. Single-edge-notch 3-point-bending (SEN-3PB) test, following the ASTM D5045-96 method, was used to obtain mode-I critical stress intensity factor (K_{IC}) of the neat epoxy and epoxy/α-ZrP nanocomposite systems. Care was taken to make sure the starter crack exhibits a thumbnail shape crack front before testing. An average of at least five specimens was used to determine K_{IC} of the samples.

Results and Discussion

Characterization of M-α-ZrP. The X-ray powder pattern of the Jeffamine intercalate shown in Figure 3 presents only the 00*l* reflections due to the severe preferred orientation exhibited by the Jeffamine intercalate resulting from its layered structure. Ten orders of 00*l* were present and these were averaged to obtain the basal spacing of 73.3 Å. This value is almost 10 times the value of α-ZrP interlayer spacing (7.6 Å).

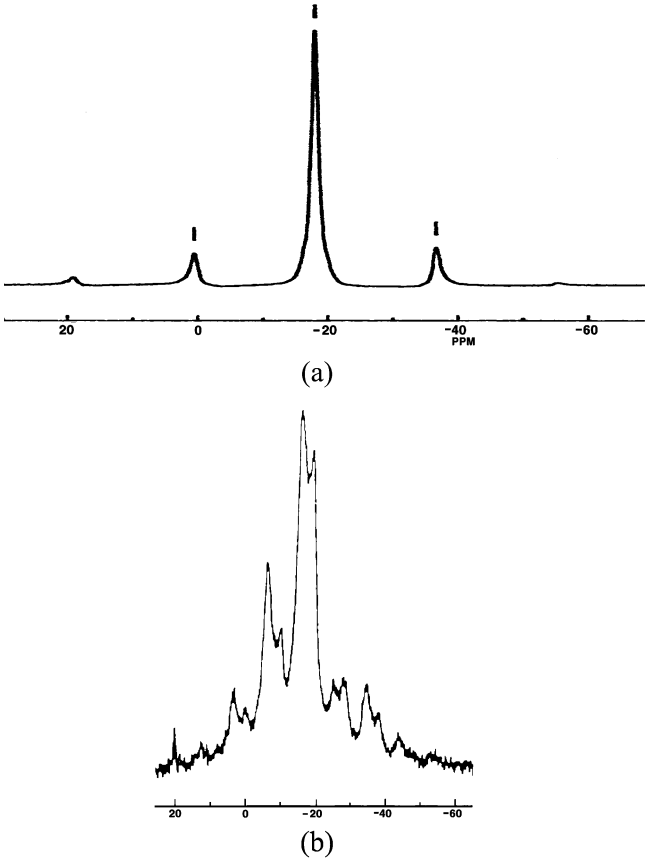

Figure 4. (a) ^{31}P NMR of α-zirconium phosphate. The signal is at −18.9 ppm. (b) ^{31}P NMR of an α-zirconium phosphate intercalated with M715. Two signals at −16 and −18 ppm show that a portion of the phosphate has reacted with the amine.

The intercalate, being a "gel", where the excess Jeffamine was not able to be washed out, made it very difficult to analyze. In a previous paper, we studied the intercalation of different Jeffamines in α-ZrP.[35] For example, thermogravimetric analysis and elemental analyses on the α-zirconium phosphate intercalated with Jeffamine M300 (this compound formula is $C_7H_{15}O$-$(((CH_3CH(CH_3)O)_2CH_2CH_2NH_2))$ allowed us to conclude that only 1 mol of the Jeffamine M300 was intercalated into 1 mol of α-zirconium phosphate. Structural evidence confirms this hypothesis. It is well-known that even when as little as 1 mol of amine is intercalated into α-ZrP, a bilayer is formed.[30] Presumably only every other −POH group interacts with an amine molecule. However, no interpenetration occurs but rather the angle at which the amine is inclined to the layers is smaller, decreasing the interlayer distance. In the case of M715 intercalation the very large interlayer spacing also indicates the presence of a bilayer with no interpenetration.

The ^{31}P NMR spectra of the M-α-ZrP intercalate (Figure 4) shows two peaks at −18 and −16 ppm against the −18.9 ppm before the intercalation, which suggests that only a portion of the phosphate group is reacted with the amine (a shift of 2 ppm). Similar shifts have been observed on intercalation of *n*-alkylamines.[36] This

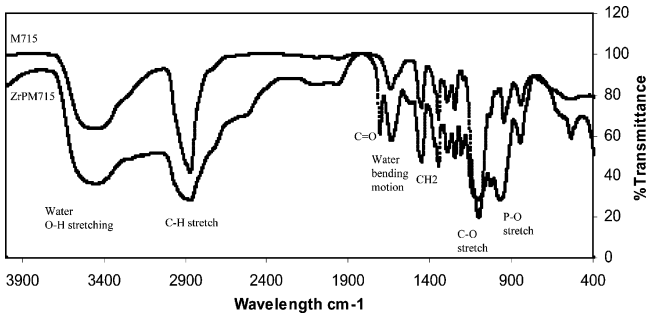

Figure 5. Infrared spectrum of Jeffamine M715 and α-zirconium phosphate intercalated with Jeffamine M715.

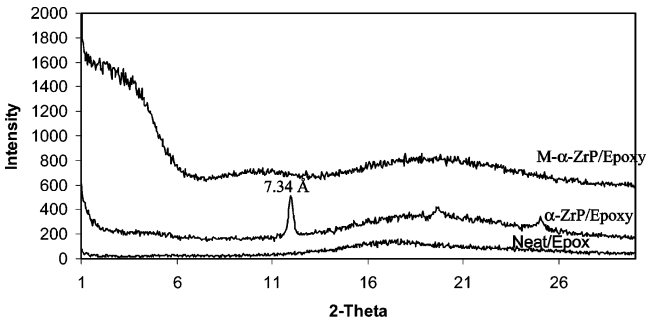

Figure 6. X-ray diffraction powder pattern of (a) α-ZrP/epoxy, (b) neat/epoxy, and (c) M-α-ZrP/epoxy.

supports the previous conjecture of the bilayer structure formation with every other −POH groups.

The infrared spectra shown in Figure 5 present the following bands: 3448, 2873, 1710, 1639, 1456, 1106, and 971 cm^{-1}, which are assigned as water (O−H stretching), C−H stretching, C═O stretching due to the remaining MEK trapped in the gel, water bending motion, $-CH_2$, C−O stretching from the ether, and P−O stretching, respectively. Bands corresponding to protonated nitrogen were not detected. These bands are located at 3400−3100 cm^{-1} for stretch and 1520 cm^{-1} for bend and are difficult to detect. Thus, it can be assumed that the amine is hydrogen-bonded to the free hydroxide of the phosphate group. Comparison of the M715 spectrum with the α-ZrP intercalate shows that all the important bands of M715 are also present in the ZrP M715 spectrum. It is also notable that the three sharp bands in the OH stretching region of α-ZrP have merged into a single broad band and the five P−O bands in the α-ZrP spectrum are reduced to three in the intercalate.[37]

Characterization of M-α-ZrP/Epoxy Nanocomposite. Figure 6 presents respectively the powder patterns of M-α-ZrP/epoxy, neat/epoxy, and α-ZrP/epoxy. The X-ray diffraction powder pattern of the M-α-ZrP/epoxy nanocomposite shows broad humps around 2°, 10°, and 20° in 2θ, which is different from M-α-ZrP. This powder pattern exhibits the amorphous nature of the nanocomposite material. The first two humps can be assigned to the inorganic matrix, while the third large broad hump is assigned to the epoxy matrix. In the case of α-ZrP/epoxy the powder pattern shows a peak at 7.34 Å; this value was 7.58 Å in the starting α-ZrP. This change in the interlayer spacing is probably due to the loss of the water molecule, induced by the heating

(36) MacLachlan, D. J.; Morgan, K. R. *J. Phys. Chem.* **1990**, *94*, 7657. (b) MacLachlan, D. J.; Morgan, K. R. *J. Phys. Chem.* **1992**, *96*, 3459.

(37) Clearfield, A. *Inorganic Ion Exchange Materials*; Clearfield, A., Ed.; CRC Press: Boca Raton, FL, 1982; p 5.

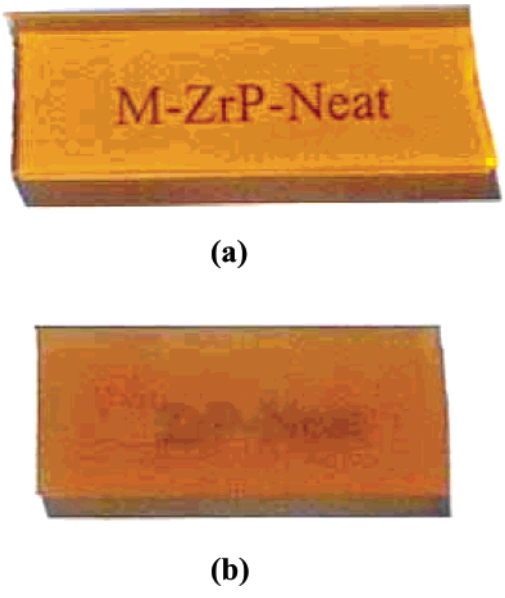

Figure 7. Photographs of (a) transparent M-α-ZrP/epoxy and (b) opaque α-ZrP/epoxy samples.

during the polymerization process, and shows that the layer structure has not been disturbed by the epoxy.

To directly investigate the dispersion and the state of intercalation/exfoliation of α-ZrP in the epoxy matrix, OM, SEM, and TEM observations were performed. The SEM images of α-ZrP powder before intercalation are shown in Figure 2 and showed aggregated primary particles having sizes in submicrometer range. After intercalation α-ZrP particles with the monoamine and dispersion in epoxy, the nanocomposite panel becomes transparent with a slight yellowish color induced by surface oxidation, which is commonly found in cured epoxies. The M-α-ZrP/epoxy panel showed no visible aggregation (Figure 7a). In comparison, the composite α-ZrP/epoxy is opaque and dark-brown in color, indicating the existence of submicrometer size α-ZrP aggregates (Figure 7b).

To ensure that no M-α-ZrP aggregates are present and the overall dispersion of M-α-ZrP in epoxy is uniform, additional OM and SEM investigations were performed. Even after exhaustive examination at high magnifications, no signs of α-ZrP aggregates were found in the matrix. Therefore, no OM and SEM micrographs are presented here since their morphologies investigated are simply featureless.

TEM observation of M-α-ZrP/epoxy shows widespread exfoliated α-ZrP particles in the epoxy (Figure 8). The state of dispersion and exfoliation of α-ZrP particles in the epoxy matrix is uniform throughout the sample. It is noted that the plane view images of the α-ZrP particles, that is, the TEM thin section is parallel to the α-ZrP platelet surface, are observed. It is also noted that, with only 1.9 vol % of α-ZrP inorganic loading, the area fraction of α-ZrP in epoxy appears to be much higher than 1.9 vol %. This apparent higher percentage of α-ZrP particles in the micrograph is due to the tilting of the α-ZrP platelets from the plane of the TEM thin section, and to the good dispersion and exfoliation of the α-ZrP in epoxy. In contrast, the TEM micrograph of α-ZrP/epoxy clearly shows aggregated α-ZrP layer structures, exhibiting much lower apparent

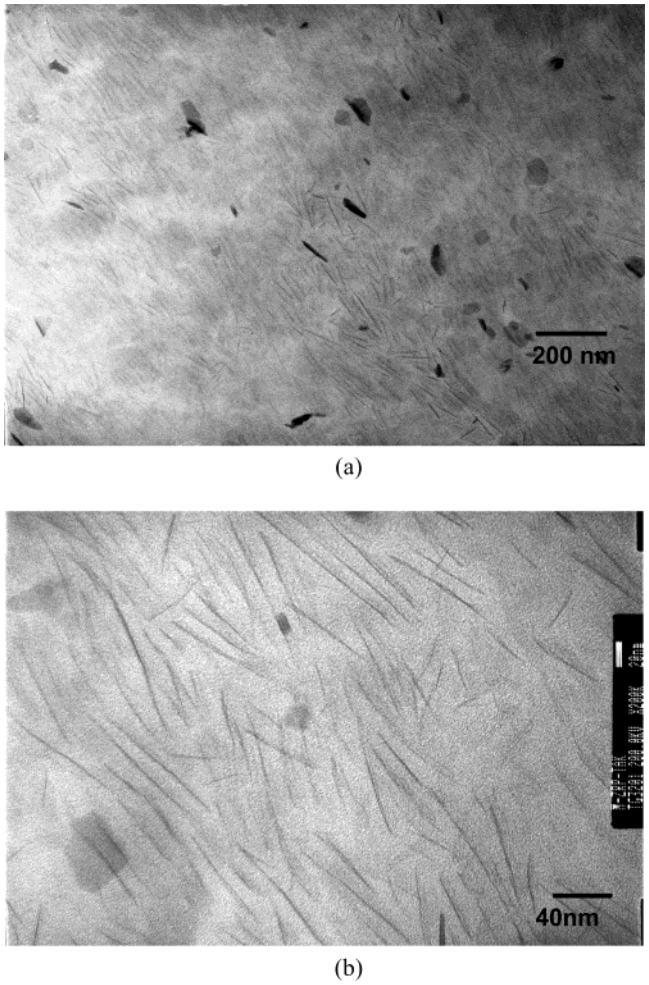

Figure 8. TEM of M-α-ZrP/epoxy showing (a) low magnification and (b) high magnification of uniform dispersion and exfoliation of α-ZrP Layers.

area fraction than that of the M-α-ZrP/epoxy system (Figure 9).

The aspect ratio of the α-ZrP layer can also be obtained by dividing the observed length of each α-ZrP layer by the thickness of the α-ZrP layer (0.75 nm). The estimated aspect ratio of the α-ZrP ranges from about 100 to 200. Because only simple hand stirring was required to mix the polymer with the M-α-ZrP, almost no fracture of the particles occurred. Another interesting finding of the exfoliated α-ZrP is that α-ZrP platelet structure does not bend or curve (Figure 8), as opposed to the curved clay structure frequently observed in epoxy nanocomposites.[7] This implies that the α-ZrP structure is more rigid than clay since they both have approximately the same thickness and aspect ratio.

Dynamic Mechanical Behavior. The glass transition temperature (T_g) of the DGEBA/DDS epoxy system is significantly decreased by the addition of M-α-ZrP. This value drops from 227 °C in the case of neat epoxy to 90 °C for the M-α-ZrP/epoxy (Figure 10). Trianfillidis et al.[38] also observed a drop in T_g when they used Jeffamine D2000 as a surface modifier for an epoxy–clay nanocomposite; this drop was attributed to the

(38) Trianfillidis, C. S.; LeBaron, P. C.; Pinnavaia, T. J. *Chem. Mater.* **2002**, *14*, 4088.

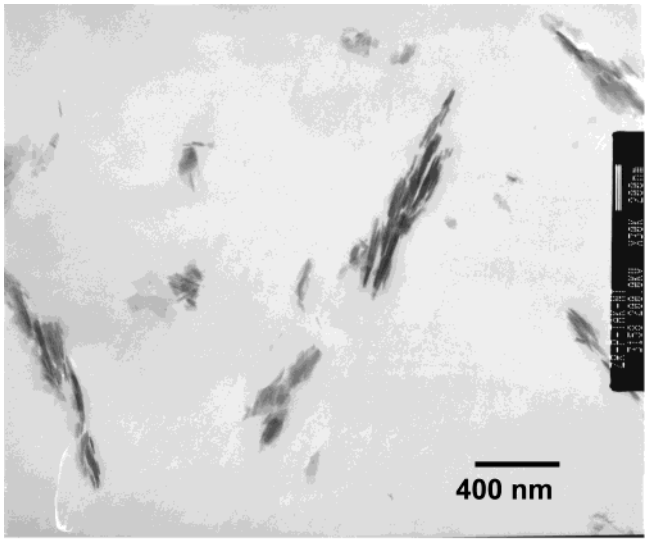

(a)

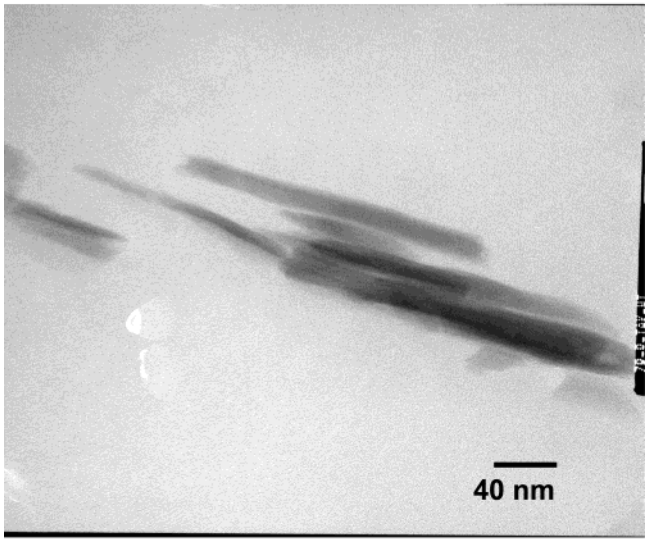

(b)

Figure 9. TEM of α-ZrP/epoxy showing (a) low magnification and (b) high magnification.

large number of propylene oxide segments in D2000. The drastic difference observed in M-α-ZrP/epoxy is likely due to the unintended reactions between the excess amount of monoamine and DGEBA epoxy. This excess monoamine M715 renders the formation of many dangling chain ends in the cured epoxy network. This speculation is supported by directly adding monoamine M715 to the DGEBA/DDS system before curing. Upon curing, the monoamine-modified DGEBA/DDS (M/epoxy) shows a significant drop in T_g, from 227 °C down to 68 °C. To make a fairer comparison, the properties of M/epoxy are compared to those of the M-α-ZrP/epoxy nanocomposite system. In this case, the T_g of M/epoxy is significantly increased from 68 to 90 °C after the addition of M-α-ZrP. However, the quantity of the monoamine M715 involved in the M-α-ZrP/epoxy curing process responsible for the significant drop in T_g is still uncertain. Therefore, it is unclear if indeed the presence of exfoliated α-ZrP actually leads to a greatly enhanced T_g in the nanocomposite, as compared to M/epoxy. This issue is currently being addressed by altering the level of monoamine and the type of surface modifiers utilized. The results will be published in a separate paper.

In the case of using unmodified α-ZrP for reinforcement, the DMA plot shows that there is no shift in T_g for the α-ZrP/epoxy system. The storage moduli of the α-ZrP/epoxy system are only slightly higher than those of DGEBA/DDS throughout the temperature range studied (Figure 10). This suggests that without surface modification, α-ZrP would act as an ordinary filler.

It is interesting that the storage modulus, G', increases more significantly at a temperature above T_g than at temperatures below T_g. In comparison to M/epoxy, the addition of M-α-ZrP to epoxy, the storage modulus, G', of the M/epoxy matrix at 25 °C is only increased from 1.03 to 1.38 GPa. However, a significant increase of the rubbery plateau modulus from 2.90 to 15.8 MPa is observed at temperatures above their respective T_g values. The 4.5 times increase in rubbery plateau modulus (Table 2) is probably because the rigid α-ZrP particles serve as physical cross-linkers to elevate the rubbery plateau modulus of the epoxy.[2,7] It is also possible that the significant increase in rubbery plateau modulus is due to the decreased amount of free monoamine in the epoxy matrix due to the adsorbed, immobile monoamine molecules on the α-ZrP surfaces.

Most interestingly, the increase in G' due to the presence of α-ZrP diminishes as the temperature decreases and becomes nondistinguishable with the neat epoxy when the temperature approaches the γ-relaxation peak of the epoxy, that is, about −80 °C. The recent molecular dynamics modeling work of Gersappe[39] suggests that the above phenomenon can be explained based on the comparable sizes and mobility between the matrix molecule and the nanofiller. The ability of the nanofiller to carry and redistribute the applied stress field depends strongly on the mobility and the size of the nanofiller. As a result, the more mobile the nanofiller is, the easier for the nanofiller to contribute to the stiffening of the matrix. Since the nanofiller is small and can be easily mobilized by the surrounding mobile molecules, the stiffening effect would be maximized when the temperature is above T_g and minimized when the temperature is below the γ-relaxation peak.

It is also worth noting that the magnitude of the tan δ damping curve of the epoxy is greatly reduced throughout the temperature range investigated when exfoliated α-ZrP is present (Figure 10). This suggests that the exfoliated α-ZrP nanofiller hinders the energy dissipation process of epoxy molecules. Thus, α-ZrP may be in motion with the neighboring epoxy molecules at a similar time scale and length scale. As a result, the presence of α-ZrP can hamper the deformation of epoxy, leading to increased modulus. This effect, again, is more pronounced when the temperature is around or above T_g. In this case, a significant increase in T_g is observed for the α-ZrP-modified epoxy.

The above argument seems reasonable since the molecular size of the epoxy, that is, the distance between cross-links in this case, is about 10−20 nm. When the filler size is far greater than the molecular size, the conventional composite principle would take effect, as

(39) Gersappe, D. *Phys. Rev. Lett.* **2002**, 89−058301.

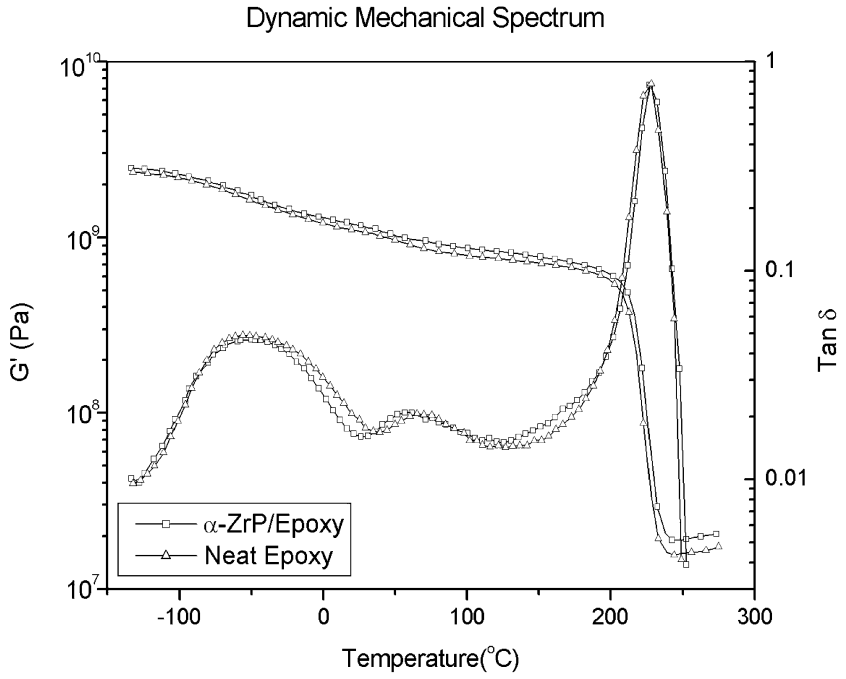

(a)

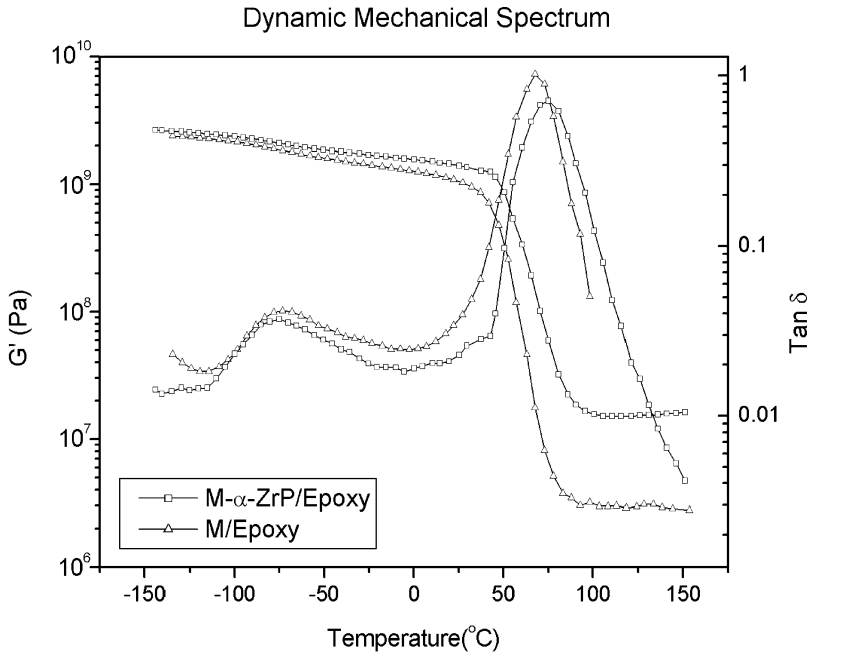

(b)

Figure 10. DMA of (a) neat and α-ZrP/epoxy, (b) M/epoxy, and M-α-ZrP/epoxy systems.

Table 2. DMA Results of α-ZrP−Epoxy Nanocomposites

	neat	M/epoxy	M-α-ZrP/ epoxy	α-ZrP/ epoxy
T_g (°C)	227	68	90	227
G' at 25 °C (Pa)	9.69×10^8	1.03×10^9	1.38×10^9	1.17×10^9
rubbery plateau modulus (Pa)	1.55×10^7	2.90×10^6	1.58×10^7	1.99×10^7

Table 3. Mechanical Properties and Fracture Toughness

	neat	M/epoxy	M-α-ZrP/ epoxy	α-ZrP/ epoxy
modulus (GPa)	2.9	2.6	3.9	3.2
yield strength (MPa)	77.6	54.0	61.0	65.9
elongation at break (%)	4.8	13.5	1.8	2.6
K_{IC} (MPa·m$^{1/2}$)	0.80	0.83	0.77	0.79

in the case of the α-ZrP/epoxy system. Nevertheless, the actual physical origin of such unusual behavior is still not known, which warrants further research in the future. Additional designed experiments are underway to validate the above conjecture.

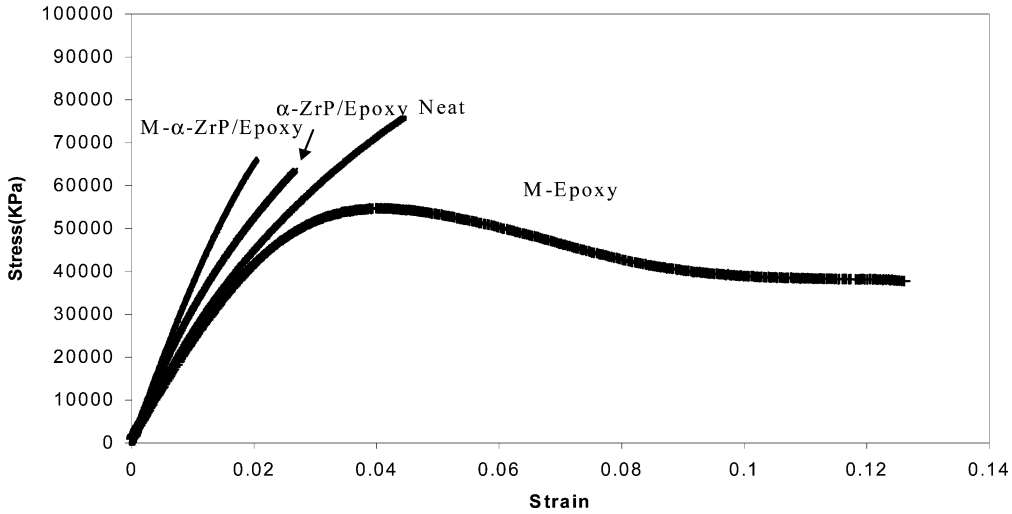

Figure 11. Tensile behavior of neat and α-ZrP-modified DGEBA/DDS epoxy systems.

Mechanical Property Characterization. With the addition of the monoamine surface modifier to DGEBA/DDS neat resin, the tensile modulus is decreased by about 10% and yield stress decreased by 30%. After the addition of 1.9 vol % M-α-ZrP to the epoxy, the corresponding properties are increased by 50% and by 10%, respectively (Table 3). The addition of M-α-ZrP to epoxy substantially increases the tensile modulus, while the elongation at break decreases significantly (Figure 11). This big drop in elongation-at-break is possibly caused by the low molecular mobility of the epoxy network structure induced by the presence of the rigid, immobile α-ZrP platelet structure, as evidenced by the significantly suppressed damping behavior in the nanocomposite (Figure 11). This is also why α-ZrP is effective in stiffening the epoxy matrix.

Mode-I critical stress intensity factor, K_{IC}, values from the SEN-3PB tests show that the fracture toughness is not significantly changed by the addition of either the monoamine modifier or M-α-ZrP (Table 3) since epoxy resin is inherently brittle and/or notch-sensitive. This finding is consistent with our earlier study on clay-filled epoxy nanocomposites systems.[7] This implies that when the nanofiller phase is well-dispersed and in small quantities, it would not act as defects to cause premature failure of the epoxy matrix.

The present research clearly shows that α-ZrP-based epoxy nanocomposites are ideal for gaining fundamental knowledge on the physics of how and why nanoparticles alter the physical and mechanical properties of polymer matrixes. The versatility and simplicity of α-ZrP synthesis to control the surface functionality, size, and aspect ratio of α-ZrP particles would allow the establishment of unambiguous fundamental relationships between nanoparticle material parameters and the physical and mechanical properties of polymer nanocomposites. We are currently working on altering the aspect ratios, sizes, and surface functionalities of α-ZrP to further investigate how and why nanofillers change the properties of polymers.

Conclusion

M-α-ZrP with wide interlayer spacing has been successfully prepared using commercially available monoamines intercalate. The intercalate is hydrogen-bonded to the host and exhibits a bilayer structure into the interlayer spacing. Uniformly dispersed and exfoliated α-ZrP-based epoxy nanocomposites were prepared. The mechanical property study of M-α-ZrP/epoxy nanocomposites shows that rubbery plateau modulus of the M-α-ZrP/epoxy nanocomposite is about 4.5 times higher than that of the M/epoxy. The tensile modulus of the M-α-ZrP/epoxy nanocomposites is increased by 50% of the reference epoxy, while the ductility is decreased drastically. The fundamental physics behind the change in mechanical property of the nanocomposite was discussed.

Acknowledgment. The authors would like to acknowledge Vladimir Bakhmutov for collection of the NMR spectra and Deyuan Kong for her help in the interpretation of the infrared spectra. Financial support from The Defense Logistic Agency (SP0103-02-D-0024), State of Texas ARP Grant (32525-73130), NSF Grant No. DMR 0080040, and the R. A. Welch Foundation, Grant No. A673, are greatly appreciated.

CM030441S